

Ion-dependent DNA Configuration in a Bacteriophage Capsid

Pei Liu¹, Javier Arsuaga², M. Carme Calderer¹, Dmitry Golovaty³, Mariel Vasquez², and Shawn Walker⁴

¹School of Mathematics, University of Minnesota, Twin Cities, Minnesota, 55455

²Department of Molecular and Cellular Biology, and Department of Mathematics, University of California Davis, Davis, California 95616

³Department of Mathematics, The University of Akron, Akron, OH, 44325

⁴Department of Mathematics, Louisiana State University, Baton Rouge, Louisiana 70803

September 17, 2020

Abstract

The long DNA chain of a bacteriophage is closely packed inside of the capsid, forming a hexagonal chromonic liquid crystal structure. Experiments have confirmed the DNA configuration is sensitive to the salt conditions. In this article, we propose a mathematical model to describe the salt-dependent DNA configuration in a bacteriophage capsid. With the total free energy of the system combining the liquid crystal free energy, the electrostatic energy and the elastic energy, the DNA and salt distribution is determined as the energy minimizer, governed by a highly nonlinear second order PDE. We develop a numerical approach based on the energy gradient flow to simulate the salt-dependent DNA configuration. Our numerical results show good agreement with existing experiments and molecular simulations.

1 Introduction

A bacteriophage is a virus made of a protein capsid that encapsulate its DNA (or RNA) genome, which have been widely used in a variety of applications such as phage therapy [1], food industry [2], drug discovery [3, 4], etc. A bacteriophage can infect certain types of bacteria by ejecting its genome into the host bacteria and then replicates itself within the host. It is very important to notice that the size a bacteriophage is usually at the order of $10nm$ while its genome length is at the order of $10\mu m$. Since the length of genome is significantly larger than the size of the capsid, thus the DNA is tightly packed and oriented, forming a hexagonal chromonic liquid crystal phases [5], which has been observed and confirmed by various of experimental and theoretical studies since 1980s [6, 7, 8, 9, 10, 11, 12, 13, 14, 15]. The bacteriophage DNA occupies almost all the volume of the capsid, with background water and ions to mediate the energy cost to pack the DNA in. Figure 1(a) sketches the DNA orientation on a cross-section that is parallel to the DNA axial direction. The cross-section perpendicular to the axial direction presents a hexagonal lattice structure, where each lattice represents the intersection of the DNA chain with the plane, as shown in Figure 1(b). Understanding the configuration of the DNA in the capsid is the foundation to study the bacteriophage properties, such as packing and ejection dynamics, as well as applications like virus design and phage therapy.

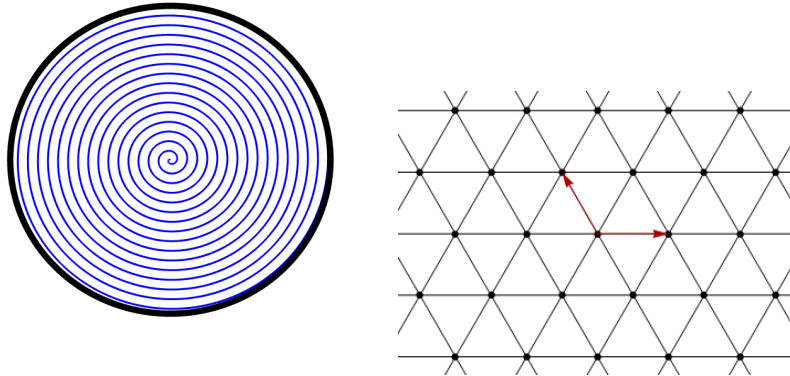


Figure 1: Configuration of packed DNA in a bacteriophage capsid. (a): Side view parallel to the axial direction. The black circle represents the capsid membrane, the blue curve describes the orientation of the DNA chain. (b): Side view perpendicular to the axial direction, each dot represents the intersection of the DNA strand with the cross-section. These dots locally behaves like a hexagonal lattice structure, while the intrastrand distance might change in space.

Although there are lots of experimental measurements on the DNA structure in the bacteriophage capsid, our understanding is still very limited without a valid first-principle model, which could match the experimental observations. Molecular simulations have been widely applied to the study the DNA packing. For example, [16] used Monte-Carlo method, [17, 18] used Brownian dynamics and [19] used Molecular dynamics. Despite the advantage of these molecular based methods, which could describe the discrete DNA strands directly and capture almost all the information about the DNA configuration, these methods are limited in the size of the capsid and the length of DNA strand, due to the high computational cost in evaluating the pairwise interaction between molecules. Recently, in [5], the authors proposed a mechanical model to study the structure of DNA encapsidation. The DNA molecules are described using the hexagonal liquid crystal, with an order parameter s to characterize the ordered packing near the capsid membrane and the disordered core region. Three main mechanisms have been discussed: entropy, bending of the DNA molecule and self-repulsion between DNA molecules. The numerical results show that, the director field \vec{n} is almost identical to the unit vector \vec{e}_θ in the cylindrical coordinate. The discrete DNA strand is then revealed by a piecewise-smooth curve using the level curve given by the direction field and the displacement vectors. Following this approach, we now focus on understanding the effect of ions to the DNA configuration and capsid properties.

The DNA chain itself is negative-charged, with a line density of about $6e/nm$ where e is the elementary charge. The aqueous environment with high ionic concentration plays an essential role in screening the electrostatic repulsion and neutralizing the overall charge distribution. Experiments and molecular simulations have shown the encapsidated DNA structure is sensitive to and can be controlled by the ionic conditions. For example, at high concentrations of spermidine, DNA condensation could happen which significantly increases the shear stresses of the DNA and reduces the pressure inside the capsid [19]. On the other hand, with increasing salt concentration, the spacing between two DNA strand is reduced, with relatively lower contribution from the DNA self-repulsion and bending energy [20].

There are mainly two mechanisms for the salts to affect the DNA configuration. The first one is through the mean-field electrostatic interaction, which could be described by the Poisson-Boltzmann theory. The other one is by changing the DNA persistence length, which is beyond the mean-field description of the electrostatics and can be taken into account through the Debye-Hückel theory with charge renormalization. In literature, there are various formulas about the salt-

dependent persistence length: (a) the Odijk–Skolnick–Fixman (OSF) model [21, 22] is valid for high ionic strengths; (b) the OSF-Manning formula [23] is a correction to low ionic concentration; (c) the Netz-Orland model agrees with a wide range of experimental data using two fitting parameters [24]; (d) an interpolation formula with four fitting parameters works for the whole ionic strength range [25]. In this work, considering the ionic solutions in biological systems are usually not dilute, it is straightforward and sufficient for us to employ the OSF model.

Besides the contribution from the electrostatics, we use the Oseen–Frank energy to describe the bending energy of this hexagonal chromonic liquid crystal structure, and introduce the Lenard–Jones energy to account for the interaction between nearby DNA strands. In this article, we propose a simple continuum model to help understanding the packing configuration of a long DNA chain inside a confined domain as well as the role of ionic conditions. Comparing with experimental and molecular simulation results in literature, our model is very efficient and is able to capture most of the quantitative behavior, and even quantitatively.

2 Model

The bacteriophage capsid is described as a rigid sphere of radius r_0 ,

$$\mathcal{B} = \{(r, \theta, z) \mid -r_0 \leq z \leq r_0, 0 \leq \theta < 2\pi, 0 \leq r \leq \sqrt{r_0^2 - z^2}\}. \quad (1)$$

Here (r, θ, z) is the cylindrical coordinate. The DNA chain orients along the z -axis, as shown in Figure 1(a). For simplicity, we assume the (tangent) director $\vec{n} = \vec{e}_\theta$, which is shown to be a good approximation in [5]. Then the system becomes homogeneous in θ . The intersection of the DNA with the $r - z$ plane is a hexagonal lattice, as shown in Figure 1(b). The cross-sectional density is a function in space, denoted as $m_0(r, z)$. Thus, the concentration of DNA molecules is $c_0(r, z) = \eta m_0(r, z)$, where η is a constant representing the line number density along the DNA chain. There are N ionic species in the system, whose valence and concentration distribution are denoted as z_i and $c_i(r, z)$, $1 \leq i \leq N$, respectively. The environment and the ionic conditions are described within a large cylinder

$$\Omega = \{(r, \theta, z) \mid -L \leq z \leq L, 0 \leq \theta < 2\pi, 0 \leq r \leq L\}. \quad (2)$$

Then the total free energy of the system is,

$$\begin{aligned} E_{cap}[c_i(r, z)] &= \int_{\mathcal{B}} k_3 |\vec{n} \times \nabla \times \vec{n}|^2 dx + \frac{1}{2} \int_{\Omega} \sum_{i=0}^N z_i e c_i \phi dx \\ &+ k_B T \int_{\Omega} [\gamma c_0 \log c_0 + \sum_{i=1}^N c_i \log c_i] dx + \int_{\mathcal{B}} f(c_0) dx. \end{aligned} \quad (3)$$

The first term comes from the Oseen–Frank free energy, describing the bending energy of the DNA strands. It should be noted the energy from splay and twist vanishes because $\vec{n} = \vec{e}_\theta$. The bending coefficient k_3 is proportional to the number density of DNA strands and its persistence length [26, 27]:

$$k_3 = k_B T \ell_p m_0. \quad (4)$$

The dependence of the DNA persistence length to the ionic condition is modeled using the OSF theory,

$$\ell_p = \ell_0 + \frac{q^2}{16\pi \sum_{i=1}^N z_i^2 e^2 c_i}. \quad (5)$$

Here ℓ_0 is a constant, q is the DNA line charge density.

The second term in Eq. (3) describes the electrostatic energy. ϕ is the mean electrical potential, given by Poisson's equation:

$$-\epsilon \nabla^2 \phi = \sum_{i=0}^N z_i e c_i. \quad (6)$$

Here ϵ is the dielectric coefficient. $z_0 = q_0/(\eta e)$ describes the valence of the DNA monomers. The boundary condition is Dirichlet $\phi = 0$ on $\partial\Omega$, which describes the overall charge neutrality in the large box Ω .

The third term in Eq. (3) comes from the entropy from both DNA and all ionic species. Since DNA is polymer, unlike the mobile ions, there should be a weight constant γ . On the other hand, the distribution of DNA strands is homogeneous in θ direction, forming a two-dimensional structure on the $r-z$ plane. The entropic density of this two-dimension distribution is proportional to $2\pi r m_0 \log m_0$. Here $2\pi r$ comes from the length (or height) of the two-dimension structure, which is the circumference of the DNA strands of radius r . This expression is equivalent to the entropy of DNA in equation (3).

The fourth term in Eq. (3) describes the elasticity between DNA strands inside of the capsid. Considering the fact that the DNAs are tightly packed, we introduce the Lenard-Jones repulsion, $f(c_0) \propto \frac{c_0}{d^{12}}$. Using the hexagonal lattice structure, the distance d between the DNA stands satisfies $d^2 \propto \frac{1}{c_0}$. So we propose,

$$f(c_0) = \alpha c_0^7. \quad (7)$$

Here α is a coefficient controlling the strength of the repulsion.

Now the total energy is simplified as,

$$\begin{aligned} E_{cap}[c_i(r, z)] &= \int_{\mathcal{B}} \frac{k_3}{r^2} dx + \frac{1}{2} \int_{\Omega} \sum_{i=0}^N z_i e c_i \phi dx \\ &+ k_B T \int_{\Omega} [\gamma c_0 \log c_0 + \sum_{i=1}^N c_i \log c_i] dx + \int_{\mathcal{B}} \alpha c_0^7 dx. \end{aligned} \quad (8)$$

The equilibrium distribution is then obtained by minimizing the total energy, subject to the following constraint conditions,

$$\begin{cases} \int_{\Omega} c_i dx = N_i, & i = 0, 1, \dots, N; \\ \int_{\mathcal{B}} c_0 dx = N_p. \end{cases} \quad (9)$$

These constraints describes the fact that, the capsid membrane is permeable to ions, but not the DNA. In reality, the DNA can only go through the motor protein during the packing or ejection process, which is not the aim of this article.

We first compute the chemical potential of DNA,

$$\mu_0 = \frac{\delta E_{cap}}{\delta c_0(r, z)} = \begin{cases} z_0 e \phi + \gamma k_B T (\log c_0 + 1) + \frac{\ell_p}{\eta r^2} + 7\alpha c_0^6, & \text{in } \mathcal{B}; \\ z_0 e \phi + \gamma k_B T (\log c_0 + 1), & \text{in } \Omega/\mathcal{B}. \end{cases} \quad (10)$$

The chemical potentials of ions are,

$$\mu_i = \frac{\delta E_{cap}}{\delta c_i(r, z)} = \begin{cases} z_i e \phi + k_B T (\log c_i + 1) - \frac{k_B T c_0 q^2 z_i^2}{16\pi\eta r^2 (\sum_{i=1}^N z_i^2 e c_i)^2}, & \text{in } \mathcal{B}; \\ z_i e \phi + k_B T (\log c_i + 1), & \text{in } \Omega/\mathcal{B}. \end{cases} \quad (11)$$

Since these expressions are highly-nonlinear, we cannot find an explicit form of the distributions. Instead, we define the implicit distribution of DNA through,

$$\begin{cases} z_0 e \phi + \gamma k_B T (\log c_0 + 1) + \frac{\ell_p}{\eta r^2} + 7\alpha c_0^6 = \mu_0^{b,in}, & \text{in } \mathcal{B}; \\ z_0 e \phi + \gamma k_B T (\log c_0 + 1) = \mu_0^{b,out}, & \text{in } \Omega/\mathcal{B}; \\ \int_{\mathcal{B}} c_0 dx = N_p; \\ \int_{\Omega} c_0 dx = N_0. \end{cases} \quad (12)$$

The implicit distribution of ions are,

$$\begin{cases} z_i e\phi + k_B T(\log c_i + 1) - \frac{k_B T c_0 q^2 z_i^2}{16\pi\eta r^2 (\sum_{i=1}^N z_i^2 e c_i)^2} = \mu_i^b, & \text{in } \mathcal{B}; \\ z_i e\phi + k_B T(\log c_i + 1) = \mu_i^b, & \text{in } \Omega/\mathcal{B}; \\ \int_{\Omega} c_i dx = N_i. \end{cases} \quad (13)$$

Here $\mu_0^{b,in}$, $\mu_0^{b,out}$, μ_i^b are all constants. Together with Poisson's equation (6), we obtain a closed PDE system, which is in the form of a modified Poisson–Boltzmann equation.

3 Numerical Results

In this section, we present the numerical results given by applying Eq. (13) to bacteriophages. The numerical method is summarized in Appendix.

Here we choose $\eta = 3nm^{-1}$, describing the fact that one basepair of DNA corresponds to about 0.34 nm of length along its strand [28]. The line charge density is approximately $q = 6e/nm$ [29], so that $z_0 = 2$. The dielectric coefficient is set to be the dielectric constant of water in room temperature $\epsilon = 78$. To determine the two parameters α and γ in the model, we require the contribution from each term in the total energy to be comparable with each other. In the following, $\gamma = 0.33$.

3.1 Comparison with molecule simulation

In this section, we use the same small viral capsid as in the molecular simulation performed by [19]: capsid size $r_0 = 12.5nm$ and genome length $N_0 = 4500$. All the DNA is inside the capsid thus $N_p = N_0$. The average concentration of DNA is $c_a = 3N_0/(4\pi r_0^3) = 0.55nm^{-3}$. We set $\alpha = 0.5^{-7}nm^{21}$. There are two ionic species Na^+ (or Mg^{2+}) and Cl^- in the system. The overall charge neutrality requires,

$$z_0 N_0 + z_1 N_1 + z_2 N_2 = 0. \quad (14)$$

In Figure 2, we present the DNA density and the salt densities in the $r - z$ plane. The DNA density outside of the capsid is identically zero, because there is no DNA outside of the capsid. Moreover, there is a layer close to the z -axis, where the DNA density is also very small. This is because of the high bending energy prevents the DNA to form an ordered structure. The radius of this region is about $2nm$, indicating that the DNA structure cannot be perfectly ordered in the center. In reality, some of the bacteriophages have a large cylindrical core protein, other bacteriophages have a large disorder core region where the DNA structure is not clear. This is consistent with our modeling of the ordered DNA distribution. When getting further away from the center, the DNA density becomes larger, showing the DNA prefers to stay close to the capsid membrane, mainly due to the bending energy. The contribution from the LJ repulsion prevents the DNA to be condensed at the membrane, but being nearly homogenous in the outer region. There is a sharp transition zone between the inner core and the outer region.

The distribution of Na^+ follows the distribution of DNA because the negatively charged DNA prefers to attract (or absorb) more positive charges. Since the membrane is permeable to ions, the Na^+ density is not zero but very small outside of the capsid. The distribution of Cl^- behaves in an opposite manner. It is repelled to the inner core region and outside of the capsid.

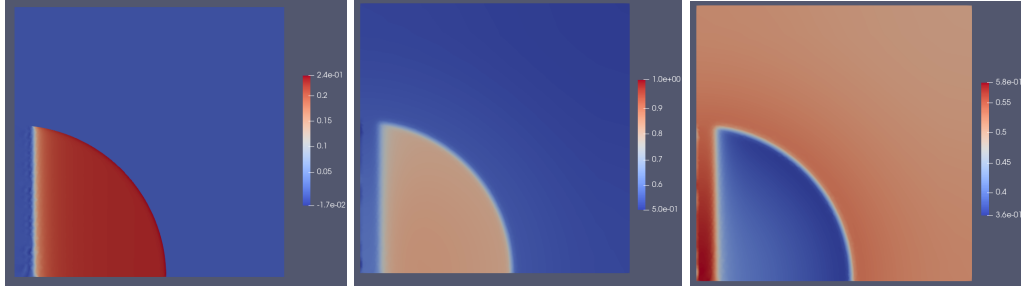


Figure 2: Number density in the $r - z$ plane. Left: DNA; Middle: Na^+ ; Right: Cl^-

To compare with [19], we plot the probability distribution of each species, as shown in Figure 3. The probability distribution is defined as,

$$P_i(r) = \frac{\int_0^\pi \int_0^{2\pi} c_i(r, \theta, \phi) r^2 \sin \phi d\theta d\phi}{\int_\Omega c_i(r, \theta, \phi) r^2 \sin \phi dr d\theta d\phi}. \quad (15)$$

Here (r, θ, ϕ) is the spherical coordinates, $r^2 \sin \phi$ is the Jacobian from Cartesian coordinate to spherical coordinate.

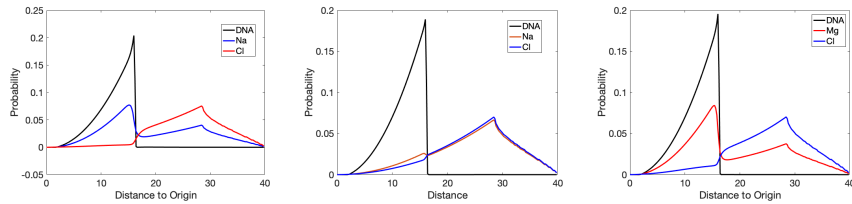


Figure 3: Left: $100mM$ NaCl ; Middle: $1666mM$ NaCl ; Right: $100mM$ MgCl_2 .

The DNA probability distribution is monotonic increasing inside of the capsid, representing the fact that the DNA density is increasing from the center to membrane. There is only one peak (local maximum) at the membrane, while [19] reported two representing two discrete layers of DNA strands. In our model, the discrete structure of DNA strands is implicitly given by the averaged concentrations. In order to capture the discrete layer structure, we need to add in the pairwise correlation energy from the hard-sphere repulsion.

Using Mg^{2+} instead of Na^+ , results in a similar curve, see Figure 2(c). This is consistent with the molecular simulation results obtained in [19]. With increasing salt concentration, the slope of the DNA curve becomes flatter. This is because the persistence length l_p becomes shorter with higher ionic strength, weakening the contribution from DNA bending. In Figure 3 (b), the Na^+ and Cl^- curves are very close, unlike the other two panels. To understand the reason, we need to take a look at the renormalized density profile as a function of r , shown in Figure 4. Here we define,

$$\rho_i(r) = \frac{\int_0^\pi \int_0^{2\pi} c_i(r, \theta, \phi) \sin \phi d\theta d\phi}{\int_0^\pi \int_0^{2\pi} \sin \phi d\theta d\phi}, \quad (16)$$

representing the average of the density $c_i(r)$ on a sphere of radius r . We can see with increasing salt concentration, the peak on the DNA curve at the capsid membrane becomes less and less significant. For the salt concentration, both inside and outside of the capsid increases. However,

Cl^- inside of the capsid increases relatively faster than outside, Na^+ inside of the capsid increases slower than outside, which makes these two curves to be similar.

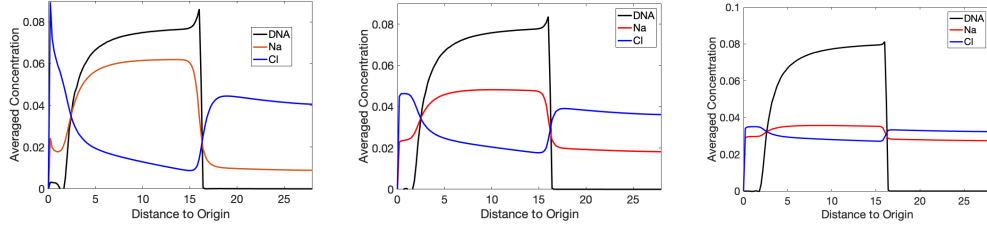


Figure 4: Average radial distributin $\rho_i(r)$ under different ionic conditions. (a): $100mM$ NaCl; (b): $300mM$ NaCl; (c): $1666mM$ NaCl.

3.2 Comparison with experiments

We now apply the model to P_4 phage of capsid size $r_0 = 22.5nm$ and genome length $N_0 = 11500$. Again $N_p = N_0$ meaning all the DNA are inside of the capsid. The average concentration of DNA is $c_a = 3N_0/(4\pi r_0^3) = 0.24nm^{-3}$. We set $\alpha = 0.2^{-7}nm^{21}$.

Figure 5(a) describes the inter-stand distance of DNA under different ionic conditions. This distance d is estimated using the hexagonal lattice structure with known density c_0 :

$$\frac{\sqrt{3}}{2}d^2 \cdot \frac{c_0}{\eta} = 1. \quad (17)$$

Here $\frac{\sqrt{3}}{2}d^2$ represents the area of a hexagon of diameter d , $\frac{c_0}{\eta} = m_0$ is the cross-sectional density. So,

$$d = \sqrt{\frac{2\eta}{\sqrt{3}c_0}}. \quad (18)$$

Since c_0 is a function of space, so d is also a function of space. Figure 5(a) presents the DNA spacing at two locations: $(22, 0)$ is near the capsid membrane, $(11, 0)$ is about half radius. Both curve show the inter-strand distance reduces with higher salt concentrations. The main reason is due to the persistent length is monotonic decreasing with the ionic strengthes, so that the DNA is easier to be packed into an ordered hexagonal structure. This result is consistent with [20].

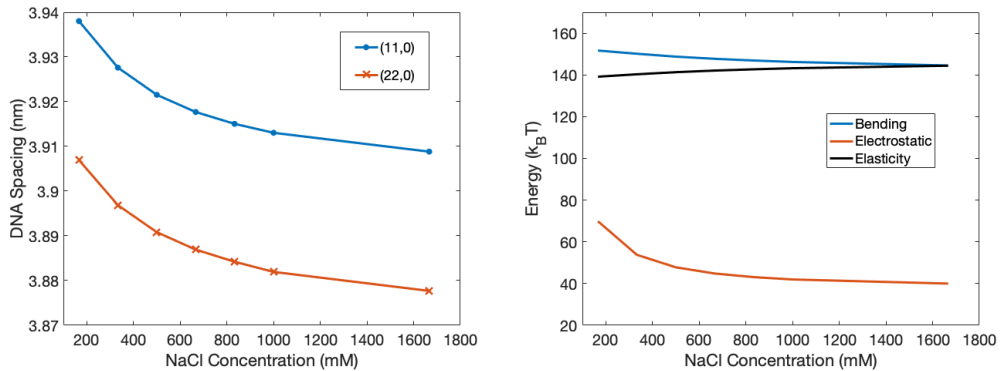


Figure 5: (a): Inter-strand distance of DNA under different NaCl concentrations; (b): The energy from bending, electrostatic and elasticity when increasing NaCl concentration.

This can also be understood from the energy point of view, by adding more salt, the overall bending energy decreases because of a smaller persistence length, and the elastic energy increases because of the smaller separation. The electrostatic energy also decreases, as shown in Figure 5(b).

4 Conclusion and Discussion

We propose an ionic model to describe the structure of the DNA in a bacteriophage capsid, under different ionic conditions. The model combines the Oseen–Frank energy from the Liquid Crystal theory with salt-dependent persistence length, the electrostatic potential energy between charges, and the elasticity between DNA strands. The agreements between the model and the existing experimental and molecular simulation results, on the DNA and ion distributions, the intra-strand DNA distance, and the energies, validates the model is capable to capture the structure of the DNA under physiological conditions. On the other hand, as a continuum model, solving the equations numerically is much faster compared with the approaches based on molecular simulations, and can be applied to large bacteriophages.

Improvements of the model can be made by taking into account these mechanisms in more detail. Although the usage of OSF theory to model the ion dependent persistence length is shown to be sufficient and successful with high ionic concentrations, extensions to lower ionic conditions can be made by employing different theories. It is also known that, there could be effective attraction between DNA strands in the presence of multi-valent ions, which means the elastic energy depends on the ionic conditions.

Appendix: Numerical Method

Due to the highly nonlinearity, nonlinear iterative method such as Newton’s method cannot guarantee the convergence. We use the gradient flow approach to solve a pseudo-time-dependent problem, which is a set of modified Poisson–Nernst–Planck equations,

$$\begin{cases} -\nabla \cdot \epsilon \nabla \phi = \sum_{i=0}^N z_i e c_i, \\ \frac{\partial}{\partial t} c_i = \nabla \cdot J_i = \nabla \cdot \left(k_B T \nabla c_i + c_i \nabla (z_i e \phi - \chi \frac{k_B T c_0 q^2 z_i^2}{16\pi \eta r^2 (\sum_{i=1}^N z_i^2 e c_i)^2}) \right), \\ \frac{\partial}{\partial t} c_0 = \nabla \cdot J_0 = \nabla \cdot \left(k_B T \gamma \nabla c_0 + c_0 \nabla (z_0 e \phi + \chi \frac{k_B T \ell_p}{\eta r^2}) \right). \end{cases} \quad (19)$$

Here $\chi = 1$ in \mathcal{B} and $\chi = 0$ in Ω/\mathcal{B} . The boundary conditions are,

$$\begin{cases} \phi = 0, \text{ on } \partial\Omega; \\ J_i \cdot \vec{e}_n = 0, \quad i = 0, 1, \dots, N, \text{ on } \partial\Omega. \end{cases} \quad (20)$$

The interface conditions on ∂B are,

$$\begin{cases} [\phi] = 0; \\ [\epsilon \nabla \phi \cdot \vec{e}_n] = 0; \\ [\mu_i] = 0; \\ [J_i \cdot \vec{e}_n] = 0, \quad i = 1, 2, \dots, N; \\ J_0 \cdot \vec{e}_n = 0; \end{cases} \quad (21)$$

It is straightforward to verify, this system satisfies,

$$\frac{d}{dt} E_{cap} = - \int_{\Omega} \sum_{i=0}^N \frac{J_i^2}{c_i} dx. \quad (22)$$

So the energy is decreasing.

To simplify, we first non-dimensionalize the equations, using $\tilde{\phi} = \beta e \phi$, $\tilde{x} = x/L_c$, $\tilde{c}_0 = c_0 L_c^3$. Here $L_c = 1nm$. For simplicity we drop all the tilde in the non-dimensional equations:

$$\begin{cases} -\nabla^2 \phi = 4\pi \ell_B \sum_{i=0}^N z_i c_i, \\ \frac{\partial}{\partial t} c_i = \nabla \cdot J_i = \nabla \cdot \left(\nabla c_i + c_i \nabla (z_i \phi - \chi \frac{c_0 q^2 z_i^2}{16\pi \eta r^2 (\sum_{i=1}^N z_i^2 c_i)^2}) \right), \\ \frac{\partial}{\partial t} c_0 = \nabla \cdot J_0 = \nabla \cdot \left(\gamma \nabla c_0 + c_0 \nabla (z_0 \phi + \chi \frac{\ell_p}{\eta r^2}) \right). \end{cases} \quad (23)$$

Here $\ell_B = \frac{e^2}{4\pi \epsilon k_B T}$ is the Bjerrum length. Using these non-dimensional quantities, the total energy is reformulated as,

$$\begin{aligned} \beta E_{cap}[c_i(r, z)] &= \int_{\mathcal{B}} \frac{c_0}{\eta r^2} \left(\ell_0 + \frac{z_0^2 \eta^2}{16\pi \sum_{i=1}^N z_i^2 c_i} \right) dx + \frac{1}{2} \int_{\Omega} \sum_{i=0}^N z_i c_i \phi dx \\ &+ \int_{\Omega} [\gamma c_0 \log c_0 + \sum_{i=1}^N c_i \log c_i] dx + \int_{\mathcal{B}} \alpha c_0^7 dx. \end{aligned} \quad (24)$$

Then we use the Implicit-Explicit scheme for the time discretization,

$$\begin{cases} \frac{c_i^{n+1} - c_i^n}{\tau} = \nabla \cdot \left(\nabla c_i^{n+1/2} + c_i^{n+1/2} \nabla \mu_{i,ex}^{n+1/2} \right), \\ \frac{c_0^{n+1} - c_0^n}{\tau} = \nabla \cdot \left(\nabla c_0^{n+1/2} + c_0^{n+1/2} \nabla \mu_{0,ex}^{n+1/2} \right) \end{cases} \quad (25)$$

Here $c_i^{n+1/2} = (c_i^n + c_i^{n+1})/2$, $\mu_{i,ex}^{n+1/2} = (3\mu_{i,ex}^n - \mu_{i,ex}^{n-1})/2$, $\mu_{i,ex}^n = z_i \phi^n - \chi \frac{c_0^n q^2 z_i^2}{16\pi \eta r^2 (\sum_{i=1}^N z_i^2 c_i^n)^2}$, $\mu_{0,ex}^n = z_0 \phi^n + \chi \frac{\ell_p}{\eta r^2}$.

For the space discretization, we use finite element method with piecewise linear elements, implemented using the firedrake package [30].

References

- [1] Janis Doss, Kayla Culbertson, Delilah Hahn, Joanna Camacho, and Nazir Barezki. A review of phage therapy against bacterial pathogens of aquatic and terrestrial organisms. *Viruses*, 9(3):50, 2017.
- [2] Lorraine Endersen, Jim O'Mahony, Colin Hill, R Paul Ross, Olivia McAuliffe, and Aidan Coffey. Phage therapy in the food industry. *Annual review of food science and technology*, 5:327–349, 2014.
- [3] Jing Liu, Mohammed Dehbi, Greg Moeck, Francis Arhin, Pascale Bauda, Dominique Bergeron, Mario Callejo, Vincent Ferretti, Nhuan Ha, Tony Kwan, et al. Antimicrobial drug discovery through bacteriophage genomics. *Nature biotechnology*, 22(2):185–191, 2004.
- [4] Lisa O'Sullivan, Colin Buttmer, Olivia McAuliffe, Declan Bolton, and Aidan Coffey. Bacteriophage-based tools: recent advances and novel applications. *F1000Research*, 5, 2016.
- [5] Shawn Walker, Javier Arsuaga, Lindsey Hiltner, M Carme Calderer, and Mariel Vazquez. Fine structure of viral dsdna encapsidation. *Physical Review E*, 101(2):022703, 2020.

- [6] Jean Lepault, Jacques Dubochet, Werner Baschong, and E Kellenberger. Organization of double-stranded dna in bacteriophages: a study by cryo-electron microscopy of vitrified samples. *The EMBO journal*, 6(5):1507–1512, 1987.
- [7] E Kellenberger, E Carlemalm, J Sechaud, A Ryter, and G De Haller. Considerations on the condensation and the degree of compactness in non-eukaryotic dna-containing plasmas. In *Bacterial chromatin*, pages 11–25. Springer, 1986.
- [8] Randolph L Rill. Liquid crystalline phases in concentrated aqueous solutions of na+ dna. *Proceedings of the National Academy of Sciences*, 83(2):342–346, 1986.
- [9] Teresa E Strzelecka, Michael W Davidson, and Randolph L Rill. Multiple liquid crystal phases of dna at high concentrations. *Nature*, 331(6155):457–460, 1988.
- [10] Françoise Livolant. Ordered phases of dna in vivo and in vitro. *Physica A: Statistical Mechanics and its Applications*, 176(1):117–137, 1991.
- [11] Amilie Leforestier and F Livolant. Supramolecular ordering of dna in the cholesteric liquid crystalline phase: an ultrastructural study. *Biophysical journal*, 65(1):56–72, 1993.
- [12] Heung-Shik Park, Shin-Woong Kang, Luana Tortora, Yuriy Nastishin, Daniele Finotello, Satyendra Kumar, and Oleg D Lavrentovich. Self-assembly of lyotropic chromonic liquid crystal sunset yellow and effects of ionic additives. *The Journal of Physical Chemistry B*, 112(51):16307–16319, 2008.
- [13] Amelie Leforestier, Sandrine Brasilès, Marta de Frutos, Eric Raspaud, Lucienne Letellier, Paulo Tavares, and Françoise Livolant. Bacteriophage t5 dna ejection under pressure. *Journal of molecular biology*, 384(3):730–739, 2008.
- [14] Amélie Leforestier and Françoise Livolant. Structure of toroidal dna collapsed inside the phage capsid. *Proceedings of the National Academy of Sciences*, 106(23):9157–9162, 2009.
- [15] Daniel Reith, Peter Cifra, Andrzej Stasiak, and Peter Virnau. Effective stiffening of dna due to nematic ordering causes dna molecules packed in phage capsids to preferentially form torus knots. *Nucleic acids research*, 40(11):5129–5137, 2012.
- [16] Javier Arsuaga, Robert K-Z Tan, Mariel Vazquez, Stephen C Harvey, et al. Investigation of viral dna packaging using molecular mechanics models. *Biophysical chemistry*, 101:475–484, 2002.
- [17] Stephen C Harvey, Anton S Petrov, Batsal Devkota, and Mustafa Burak Boz. Viral assembly: a molecular modeling perspective. *Physical Chemistry Chemical Physics*, 11(45):10553–10564, 2009.
- [18] Andrew James Spakowitz and Zhen-Gang Wang. Dna packaging in bacteriophage: is twist important? *Biophysical journal*, 88(6):3912–3923, 2005.
- [19] Andrés Córdoba, Daniel M Hinckley, Joshua Lequieu, and Juan J de Pablo. A molecular view of the dynamics of dsdna packing inside viral capsids in the presence of ions. *Biophysical journal*, 112(7):1302–1315, 2017.
- [20] Xiangyun Qiu, Donald C Rau, V Adrian Parsegian, Li Tai Fang, Charles M Knobler, and William M Gelbart. Salt-dependent dna-dna spacings in intact bacteriophage λ reflect relative importance of dna self-repulsion and bending energies. *Physical review letters*, 106(2):028102, 2011.
- [21] Theo Odijk. Polyelectrolytes near the rod limit. *Journal of Polymer Science: Polymer Physics Edition*, 15(3):477–483, 1977.

- [22] Jeffrey Skolnick and Marshall Fixman. Electrostatic persistence length of a wormlike polyelectrolyte. *Macromolecules*, 10(5):944–948, 1977.
- [23] Gerald S Manning. A procedure for extracting persistence lengths from light-scattering data on intermediate molecular weight dna. *Biopolymers: Original Research on Biomolecules*, 20(8):1751–1755, 1981.
- [24] Roland R Netz and Henri Orland. Variational charge renormalization in charged systems. *The European Physical Journal E*, 11(3):301–311, 2003.
- [25] Annaël Brunet, Catherine Tardin, Laurence Salome, Philippe Rousseau, Nicolas Destainville, and Manoel Manghi. Dependence of dna persistence length on ionic strength of solutions with monovalent and divalent salts: a joint theory–experiment study. *Macromolecules*, 48(11):3641–3652, 2015.
- [26] Shelly Tzlil, James T Kindt, William M Gelbart, and Avinoam Ben-Shaul. Forces and pressures in dna packaging and release from viral capsids. *Biophysical journal*, 84(3):1616–1627, 2003.
- [27] WS Klug and M Ortiz. A director-field model of dna packaging in viral capsids. *Journal of the Mechanics and Physics of Solids*, 51(10):1815–1847, 2003.
- [28] George R Heath, Mengqiu Li, Isabelle L Polignano, Joanna L Richens, Gianluca Catucci, Paul OShea, Sheila J Sadeghi, Gianfranco Gilardi, Julea N Butt, and Lars JC Jeuken. Layer-by-layer assembly of supported lipid bilayer poly-l-lysine multilayers. *Biomacromolecules*, 17(1):324–335, 2016.
- [29] Robert Gilbert. *Physical biology of the cell*, by rob phillips, jane kondev and julie theriot, 2009.
- [30] Florian Rathgeber, David A Ham, Lawrence Mitchell, Michael Lange, Fabio Luporini, Andrew TT McRae, Gheorghe-Teodor Bercea, Graham R Markall, and Paul HJ Kelly. Fire-drake: automating the finite element method by composing abstractions. *ACM Transactions on Mathematical Software (TOMS)*, 43(3):1–27, 2016.